Scaling in Charge-Density-Wave Relaxation: Time-Resolved X-Ray Scattering Measurements

K. L. Ringland, A. C. Finnefrock, Y. Li, and J. D. Brock
School of Applied & Engineering Physics, Cornell University, Ithaca, New York 14853

S. G. Lemay and R. E. Thorne
Department of Physics, Cornell University, Ithaca, New York 14853
(Received 31 July 1998)

Using time-resolved, high-resolution x-ray scattering techniques, we have measured the evolution of the transverse structure of the $NbSe_3$ $\mathbf{Q}_1$ charge-density wave as it relaxes from the sliding state to the pinned state. Measurements were made at temperatures between 70 and 120 K and at electric field strengths between $2\times$ and $10\times$ the threshold for sliding. These time-dependent data are accurately described by dynamic scaling theory. [S0031-9007(99)08578-6]

PACS numbers: 71.45.Lr, 05.20.Dd, 61.10.–i

In many highly anisotropic materials, the equilibrium state at low temperatures is the charge-density-wave (CDW) state. The CDW state consists of a periodic modulation of the conduction electron density and a concomitant lattice-distortion wave (LDW) [1]. A few of these materials also exhibit non-Ohmic conduction due to a collective motion or "sliding" of the CDW. Sliding is not observed for electric fields below a threshold field due to pinning from impurities and other lattice defects [2–4]. A detailed understanding of the transition between the pinned and the sliding states requires new insight into the competition between elastic interactions and quenched random pinning fields in nonequilibrium systems. The approaches used to model this transition can be placed into two general categories: (i) scaling solutions to statistical models and (ii) solutions of the microscopic equations of motion. In this Letter, we report time-resolved x-ray scattering measurements of the evolution of the transverse structure of the CDW as it relaxes from the sliding to the pinned state and demonstrate that the relaxation kinetics are consistent with the general predictions of both approaches.

X-ray scattering is a nearly ideal probe of the CDW structure. In the simplest case, the LDW is assumed to have the form $\mathbf{u}(\mathbf{r},t) = \mathbf{u}_0 \sin[\mathbf{Q}\cdot\mathbf{r} + \phi(\mathbf{r},t)]$. Here, $\mathbf{Q} = 2k_F\hat{\mathbf{n}}$ is the CDW wave vector, k_F is the Fermi wave number, and ϕ is the phase of the CDW. This periodic distortion produces satellite peaks in the scattering near the Bragg peaks of the unperturbed crystal lattice. Near these CDW satellites, the intensity of the scattered x rays is given by

$$I(\mathbf{q},t) \sim |J_1(\mathbf{q}\cdot\mathbf{u}_0)|^2 \int d^3\mathbf{r}\, e^{i(\mathbf{q}-\mathbf{G}\pm\mathbf{Q})\cdot\mathbf{r}} e^{-g(\mathbf{r},t)}. \quad (1)$$

Here, $g(\mathbf{r},t) = \frac{1}{2}\langle[\phi(\mathbf{r},t) - \phi(\mathbf{0},t)]^2\rangle$ is the equal-time phase-phase correlation function, $J_1(x)$ is the Bessel function of order 1, $\mathbf{q}$ is the scattering vector, and $\mathbf{G}$ is a reciprocal lattice vector of the undistorted crystal. Equation (1) holds when the phase fluctuations are small with zero mean and is exact for a Gaussian probability distribution. At low temperatures, the CDW amplitude $\mathbf{u}_0$ is assumed to be constant so that $I(\mathbf{q},t)$ is completely determined by $g(\mathbf{r},t)$.

The anisotropic metal $NbSe_3$ exhibits two independent phase transitions to incommensurate CDW states at $T_1 \approx 145$ K and at $T_2 \approx 59$ K. The higher temperature transition produces satellite peaks with $\mathbf{Q}_1 \approx (0\ 0.243\ 0)$. (The crystal structure of $NbSe_3$ is monoclinic. The real space lattice constants are $a = 10.009$ Å, $b = 3.4805$ Å, $c = 15.629$ Å, and $\beta = 109.47°$ [5].) We chose to study $NbSe_3$ because its $\mathbf{Q}_1$ CDW exhibits sliding conduction and because it is available in nearly perfect, single-crystal whiskers. For this study we chose whiskers with extremely regular cross-sectional shapes, small bulk crystal mosaics, and, in the case of the pure samples, excellent mode-locking characteristics (100% at the 1/1 step and clean subharmonics) [6,7]. The macroscopic sample dimensions were approximately 2 μm × 20 μm × 5 mm. Residual resistance ratios were approximately 300 for the pure samples and 70 for the doped samples, the latter corresponding to a tantalum density of 3×10^{18} cm^{-3} [8]. Typical threshold field values were 0.08 V cm^{-1} for pure samples and 0.3 V cm^{-1} for doped samples at 120 K.

The white x-ray beam generated by the National Synchrotron Light Source (NSLS) storage ring was doubly focused at the sample position by a toroidal mirror. A monochromator consisting of two Ge(111) crystals selected 8.25-keV x rays. A set of slits produced a 0.4-mm high illuminated spot centered on the middle of the whisker (the width of the whisker sets the other dimension). The bulk crystal mosaic (0.009° FWHM) dominated the transverse resolution. The longitudinal and out-of-plane resolutions are determined by a final set of slits. The resulting resolution function is highly asymmetric and effectively integrates over the longitudinal and out-of-plane directions in Eq. (1), collapsing the three-dimensional integral to one dimension [9]. Thus, we can measure the evolution of the transverse CDW line shape, while effects due to the

 © 1999 The American Physical Society

longitudinal, position-dependent strain of the CDW in the sliding state [10–14] are integrated out.

To perform time-resolved measurements at high q resolution, we use a signal averaging technique. In this experiment, the periodic wave form of the applied electric field switches between on and off. Typical "on" fields range from $2\times$ to $10\times$ threshold. Using a multichannel scaler and an averaging memory unit, we measure the time dependence of the scattered intensity at each point in reciprocal space, integrating over enough cycles of the applied field to obtain good counting statistics in each time bin [11].

A typical time-resolved scan is shown in Fig. 1a. At early times, the CDW is sliding, and the CDW satellite is relatively broad. When the applied field is turned off (at $t = 0$, as shown in Fig. 1b), the CDW satellite shifts its position slightly, sharpens, and increases its peak intensity (Fig. 2). As shown in Fig. 1c, although the peak intensity and width change, the integrated intensity remains constant. This behavior supports the assumption that the CDW amplitude $\mathbf{u}_0$ is constant. In the doped samples, the pinned state correlation length $\ell_{\mathbf{a}^*} \approx 2100$ Å, which is roughly two-thirds of that for the zero-field-cooled state [9,15]. In general, for applied fields up to $40\times$ threshold and for temperatures between 120 and 70 K, the width of the CDW satellite in the sliding state is broader than that in the pinned state. This behavior is contrary to existing theoretical predictions and is the subject of a future publication on the structure of the pinned and sliding states. The characteristic time scale of the structural response ranges from microseconds to seconds depending on the temperature and dopant density. The shift in peak position varies from sample to sample but is insensitive to temperature or position on the sample and corresponds to a small rotation ($<0.1°$) of the CDW wave vector.

Motivated by the striking similarity between the equations describing CDW scattering and those describing surface/interface scattering [16], we begin our analysis of the kinetic data by considering scaling theories developed to describe surface growth [17–19]. Specifically, we assume that $g(\mathbf{r}, t) = r^{2\alpha} f(\frac{r}{t^{\mu}})$, where the scaling function $f(y)$ has the properties

$$f(y) = \begin{cases} \text{const} & \text{for } y \ll 1\,, \\ y^{-2\alpha} & \text{for } y \gg 1\,. \end{cases} \tag{2}$$

Using the above scaling form for $g(\mathbf{r}, t)$ and integrating over the broad resolution directions, Eq. (1) reduces to

$$I(q_\perp, t) \sim \int_0^a \cos[(q_\perp - G_\perp)x] e^{-(x/\xi)^{2\alpha}}\, dx + e^{-(t/\tau)^{2\alpha\mu}} \int_a^\infty \cos[(q_\perp - G_\perp)x]\, dx\,. \tag{3}$$

Here, $a = \xi(\frac{t}{\tau})^{\mu}$, where ξ and τ are the scaling constants for x and t, respectively. Previous x-ray scattering studies [9,15,20] have confirmed predictions [21–23] that the quenched random field destroys the long-range order of the CDW in the zero-field cooled state, producing a "roughness" exponent $\alpha = \frac{1}{2}$. Assuming $\alpha = \frac{1}{2}$, Eq. (3) becomes

$$I(q_\perp, t) \sim \frac{\xi}{1 + \xi^2(q_\perp - G_\perp)^2}[1 - e^{-(t/\tau)^{\mu}}] + \delta(q_\perp - G_\perp) e^{-(t/\tau)^{\mu}}, \tag{4}$$

where the oscillations due to the approximation have been removed. The functional form of the falling term arises from the implicit assumption that the initial state is "flat." In the growth models which inspire the above

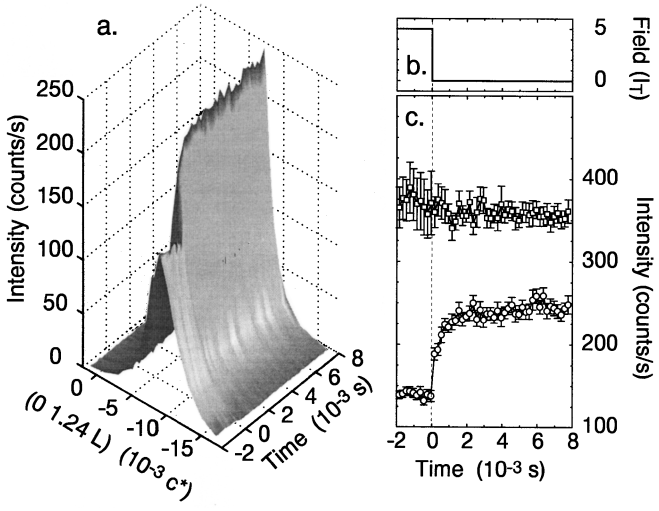

FIG. 1. (a) Pure $NbSe_3$ sample at $T = 100$ K. For $t < 0$ the CDW is in the sliding state. For $t \geq 0$ the field is off and the CDW relaxes to the pinned state. (b) Applied field. (c) Integrated (divided by 5, squares) and peak intensity (circles).

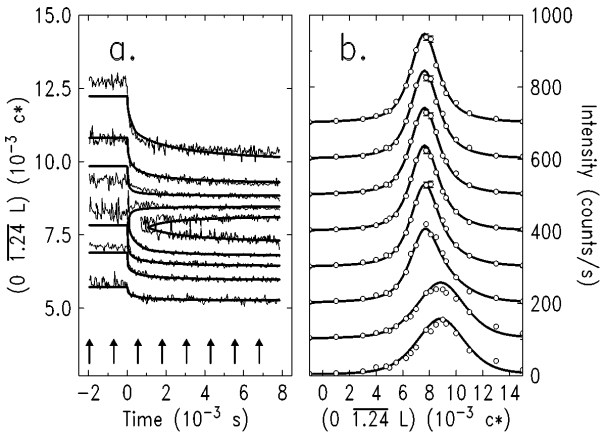

FIG. 2. (a) Contours of constant intensity: thin lines are contours of the data and thick lines are contours of the fit to Eq. (8). (b) Thick lines are slices of the two parameter fit shown in (a); circles are the data points. Early time slices are at the bottom. The arrows in (a) indicate where the cuts were taken through the data and fit.

treatment, this flatness corresponds to the initially flat substrate on which the material is grown. In the CDW system, the flatness corresponds to a perfectly ordered initial state. Thus, scaling theory predicts "stretched exponential" kinetics for the scattered intensity.

The assumption of a scaling form for $g(\mathbf{r}, t)$ may seem surprising; however, the weak pinning limit of the phase-only Fukuyama-Lee-Rice (FLR) model [24] also predicts it. To demonstrate this, consider the equation of motion for the phase in the absence of an applied field

$$\partial_t \phi(\mathbf{r}, t) = D\nabla^2 \phi + \zeta(\mathbf{r}), \tag{5}$$

where $\zeta(\mathbf{r})$ is the CDW-impurity interaction field and D is the phase diffusion constant. If the impurities have a random distribution and their interaction with the CDW is weak, the interaction field has a Gaussian distribution with $\langle \zeta(\mathbf{r})\zeta(\mathbf{r} + \mathbf{r}')\rangle = n_i V_0^2 \delta(\mathbf{r}')$, where n_i is the impurity density and V_0 is the impurity pinning strength. Although Eq. (5) is only the lowest order approximation for ϕ, it and the statistical properties of the random field correctly predict the equilibrium form of statistical quantities such as $g(\mathbf{r}, t)$ [23].

For a given $\zeta(\mathbf{r})$, Eq. (5) can be solved exactly by Fourier transforming the spatial dimensions and integrating the resulting equation of motion. This particular solution can then be averaged to calculate $\langle|\tilde{\phi}_{\mathbf{q}}(t)|^2\rangle$ [25]. For example, using the Balents-Fisher form for the initial (i.e., sliding) state [26], we obtain

$$\langle|\tilde{\phi}_{\mathbf{q}}(t)|^2\rangle = \frac{\langle|\tilde{\zeta}_{\mathbf{q}}|^2\rangle}{D^2 q^4}(1 - e^{-q^2 Dt})^2 + \frac{\langle|\tilde{F}_{\mathbf{q}}|^2\rangle}{D^2 q^4 + v_0^2 q_x^2}[1 - (1 - e^{-q^2 Dt})^2], \tag{6}$$

where $\tilde{F}_{\mathbf{q}}$ is the (renormalized) random field and v_0 is the drift velocity. $g(x, t)$ may then be written in the form $g(x, t) = g_f(x, t) + g_i(x, t)$, where $g_f(x, t)$ and $g_i(x, t)$ are, respectively, the Fourier transforms of the first and second terms in Eq. (6). Using standard techniques [27], the transform can be done analytically in one dimension. The resulting solution has the scaling form $g_f(x, t) = x^{2\alpha} f(\frac{x}{t^\mu})$, where $f(y)$ satisfies Eq. (2). A numerical implementation of the three-dimensional transformation suggests that a reasonable approximation for $g(x, t)$ is

$$g(x, t) \simeq \begin{cases} x/\xi & \text{for } x < \xi(\frac{t}{\tau})^{1/2}, \\ g_i(x) + \text{const} & \text{for } x > \xi(\frac{t}{\tau})^{1/2}, \end{cases} \tag{7}$$

where the constant is chosen to preserve the continuity of the function. As in the argument leading to Eq. (4), we break the integral in Eq. (1) into two pieces, obtaining

$$I(q_\perp, t) \simeq \frac{\xi}{1 + \xi^2(q_\perp - G_\perp)^2}[1 - e^{-(t/\tau)^{1/2}}] + I_i(q_\perp, t)e^{-(t/\tau)^{1/2}}, \tag{8}$$

where $I_i(q_\perp, 0)$ is the initial state. Thus, the kinetics predicted by Eq. (5) have exactly the same stretched exponential form as Eq. (4).

Since the decay of the initial state is dominated by the stretched exponential, we assume that there is no significant time dependence to $I_i(q_\perp, t)$ and fix its form by fitting to the sliding state for $t < 0$. We then fix the parameters ξ and $G_\perp$ by fitting to data at late times when the system has stabilized. The slight rotation of the peak position allows us to clearly distinguish contributions from the initial and final states. All of the remaining data must then be fit to only two parameters: μ and τ. To minimize the effects of our assumptions about the form of $I_i(q_\perp, t)$, we perform our final fits only to data collected at $t > \tau$. Figure 2 shows an example of a best two-parameter fit. Figure 2b shows the data collected at the time slices indicated by the arrows in Fig. 2a and the same best fit. Clearly, Eq. (8) accurately describes the kinetics of the pinning transition.

We repeated this experiment on pure samples at temperatures between 70 and 120 K and at electric field strengths between 2× and 10× threshold. The best fit values of μ and τ are shown in Figs. 3a and 4a. The results of similar measurements performed on tantalum doped samples are shown in Figs. 3b and 4b. As anticipated from the raw data, τ varies by many decades, suggesting an activated process. Although the temperature range is quite limited, an Arrenhius plot yields an activation energy $\Delta E \approx 0.2$ eV which is a few times the energy gap, $E_g \approx 0.06$ eV [28]. This result suggests a model in which the CDW relaxes by fluctuating a small volume into the normal phase. This intriguing hypothesis has significant implications for the assumption that u_0 is constant and is the subject of ongoing work. In contrast to τ, and consistent with the scaling hypothesis, μ is insensitive to temperature. Thus, we identify the exponent in our stretched

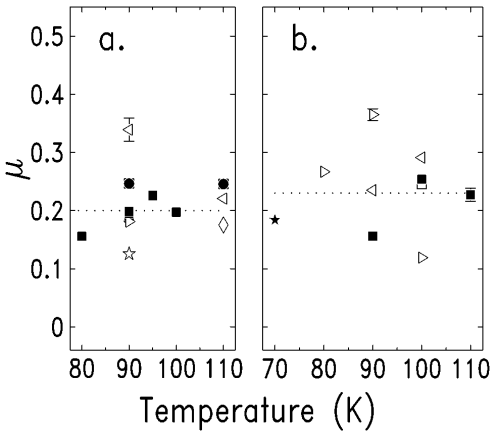

FIG. 3. Best fit values of μ for (a) pure samples and (b) tantalum doped samples. Filled and open symbols represent different samples: ○ = 10×, □ = 5×, ◁ = 4×, ▷ = 3×, ◇ = 2.5×, and ⋆ = 2× the threshold field. Dotted lines are the average values of μ.

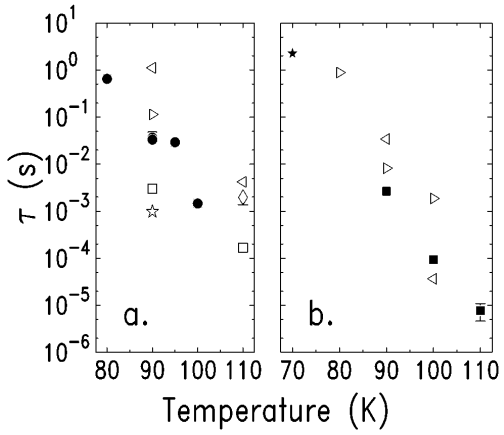

FIG. 4. Best fit values of τ for (a) pure samples and (b) tantalum doped samples.

exponential kinetics with the dynamic scaling exponent μ, with a best fit value of 0.21 ± 0.04 for the pure samples and 0.24 ± 0.06 for the doped samples (error bars are dominated by the point scatter and represent one standard deviation). Relaxing the assumption that $I_i(q_\perp, t)$ is constant in time tends to depress the value of μ even further. The validity of the scaling argument is unaffected since μ is shifted by a constant and the behavior of τ is unchanged. However, this behavior introduces additional uncertainty into the determination of μ. With this in mind, we estimate that $\mu = 0.2 \pm 0.1$.

In summary, we have shown that dynamic scaling accurately describes the relaxation data. Although the value of μ predicted by the weak pinning limit of the phase-only FLR model is inconsistent with $\mu \approx 0.2$, we have shown that dynamic scaling is a feature of a solution to a well known microscopic model of CDW dynamics. Finally, the measured value of μ now provides a test for future microscopic theories.

This research was supported by NSF Grants No. DMR-95-01119, No. DMR-98-01792, and No. DMR-92-57466. The authors thank M. Grant and J. P. Sethna for valuable discussions and J. Jordan-Sweet and S. Lamarra for technical assistance. K. L. R. acknowledges a NSF fellowship. S. G. L. acknowledges support from NSERC. A. C. F. acknowledges support from the Cornell Center for Materials Research (NSF Grant No. DMR-96-32275). X-ray data were collected on beam line X20A at the NSLS. The NSLS is supported by the U.S. Department of Energy, Division of Materials Sciences and Division of Chemical Sciences.

[1] R. E. Peierls, *Quantum Theory of Solids* (Clarendon Press, Oxford, 1955).
[2] H. Fröhlich, Proc. R. Soc. London A **223**, 296 (1954).
[3] R. M. Fleming and C. C. Grimes, Phys. Rev. Lett. **42**, 1423 (1979).
[4] N. P. Ong and P. Monceau, Phys. Rev. B **16**, 3443 (1977).
[5] J. L. Hodeau *et al.*, J. Phys. C **11**, 4117 (1978).
[6] R. E. Thorne *et al.*, Phys. Rev. B **35**, 6360 (1987); R. E. Thorne *et al.*, Phys. Rev. B **35**, 6348 (1987).
[7] M. P. Maher *et al.*, Phys. Rev. B **43**, 9968 (1991).
[8] J. McCarten, M. Maher, T. L. Adelman, and R. E. Thorne, Phys. Rev. Lett. **63**, 2841 (1989).
[9] D. DiCarlo *et al.*, Phys. Rev. B **50**, 8288 (1994).
[10] D. DiCarlo *et al.*, Phys. Rev. Lett. **70**, 845 (1993).
[11] E. Sweetland *et al.*, Phys. Rev. B **50**, 8157 (1994).
[12] M. E. Itkis, B. M. Emerling, and J. W. Brill, Phys. Rev. B **52**, R11 545 (1995).
[13] H. Requardt *et al.*, Phys. Rev. Lett. **80**, 5631 (1998).
[14] G. Kriza and G. Mihály, Phys. Rev. Lett. **56**, 2529 (1986).
[15] J. D. Brock, A. C. Finnefrock, K. L. Ringland, and E. Sweetland, Phys. Rev. Lett. **73**, 3588 (1994).
[16] S. K. Sinha, E. B. Sirota, and S. Garoff, Phys. Rev. B **38**, 2297 (1988).
[17] *Dynamics of Fractal Surfaces,* edited by F. Family and T. Vicsek (World Scientific, Singapore, 1990).
[18] A. L. Barabási and H. E. Stanley, *Fractal Concepts in Surface Growth* (Cambridge University Press, New York, 1995).
[19] H.-N. Yang, G.-C. Wang, and T.-M. Lu, *Diffraction from Rough Surfaces and Dynamic Growth Fronts* (World Scientific, Singapore, 1993).
[20] E. Sweetland *et al.*, Phys. Rev. Lett. **65**, 3165 (1990).
[21] Y. Imry and S. K. Ma, Phys. Rev. Lett. **35**, 1399 (1975).
[22] L. J. Sham and B. R. Patton, Phys. Rev. B **13**, 3151 (1976).
[23] K. B. Efetov and A. I. Larkin, Sov. Phys. JETP **45**, 1236 (1977).
[24] H. Fukuyama and P. A. Lee, Phys. Rev. B **17**, 535 (1978).
[25] J. G. Amar and F. Family, Phys. Rev. A **45**, 5378 (1992); see Appendix for a similar calculation.
[26] L. Balents and M. P. A. Fisher, Phys. Rev. Lett. **75**, 4270 (1995).
[27] B. Jancovici, Phys. Rev. Lett. **19**, 20 (1967).
[28] G. Grüner, *Density Waves in Solids* (Addison-Wesley, Reading, MA, 1994), and references therein.